UV and visible Raman study of thermal deactivation in a NO_x storage catalyst

Dairene Uy[a,*], Ann E. O'Neill[a], John Li[b], and William L.H. Watkins[b]

[a]*Physical and Environmental Sciences Department, Ford Research and Advanced Engineering, P.O. Box 2053, Mail Drop 3083, Dearborn, MI 48121, USA*

[b]*Chemical Engineering Department, Ford Research and Advanced Engineering, P.O. Box 2053, Mail Drop 3179, Dearborn, MI 48121, USA*

Received 25 November 2003; accepted 2 April 2004

In situ UV and visible Raman spectroscopy was used to characterize fresh and thermally aged NO_x storage-reduction catalysts, $Pt/Ba/Al_2O_3$. From the presence, absence, and nature of certain features in the spectra depending on aging temperature, we conclude that sintering, oxide formation, and separation of components occurred in the thermally aged catalysts. As aging temperature increased, less atomic oxygen was generated on platinum but a high temperature form of oxide or more strongly bound oxygen species was formed. This coincided with a loss of oxidation activity with aging temperature. Under UV excitation, observation of the OH stretch of physisorbed H_2O on aged $Pt/Ba/Al_2O_3$ indicated separation of Pt from γ-Al_2O_3, since this OH band was observed only on γ-Al_2O_3 (and Ba/Al_2O_3) but not on Pt/Al_2O_3. Nitrite/nitro species and NO (adsorbed on Pt) in aged $Pt/Ba/Al_2O_3$ indicate that Ba-containing particles are behaving somewhat independently from Pt and Al_2O_3, since these NO_x species are observed only on Pt/Al_2O_3 but not on fresh $Pt/Ba/Al_2O_3$ under NO + O_2 flow. Moreover, barium nitrate particles in aged $Pt/Ba/Al_2O_3$ are more crystalline, as shown by the intensity, width, and frequency of the nitrate peak, and possible photo-induced nitrite formation under UV excitation. Finally, a NO_x species with a broad peak at $\sim$330 cm^{-1} appeared on fresh but not in aged $Pt/Ba/Al_2O_3$ (or γ-Al_2O_3, Pt/Al_2O_3, and Ba/Al_2O_3) which may indicate proximity of Pt and Ba-containing particles in fresh $Pt/Ba/Al_2O_3$.

KEY WORDS: UV Raman; NO_x trap; sintering; $Pt/Ba/Al_2O_3$; atomic oxygen; thermal deactivation; platinum oxide.

1. Introduction

As internal combustion engines become more fuel-efficient and NO_x regulations more stringent, various technologies have been pursued to mitigate NO_x emissions. One such technology applicable to both lean-burn gasoline and diesel engines is the NO_x storage-reduction catalyst (NSR) or the lean NO_x trap, which Toyota introduced in the mid-1990s [1,2].

A typical NO_x trap contains an alkaline earth oxide (notably barium oxide) and precious metals dispersed on γ-Al_2O_3. The mechanism of the trap has been the subject of numerous investigations [3–11] and involves the storage of NO_x during lean exhaust gas conditions and its release as N_2 during the periodic, brief, slightly rich excursions of the engine. During lean operation where excess O_2 is present, it is believed that NO is oxidized to NO_2 over the Pt, and subsequently stored as barium nitrate. In rich conditions, the stored nitrate is reduced over the precious metals into N_2 by H_2, CO and hydrocarbons in the exhaust. However, barium oxide is unstable and transforms into carbonate upon exposure to air (which contains CO_2). Thus, the mechanism involves the reaction of carbonates to nitrates, as reported in several studies [12–15].

An effective NO_x storage material requires optimal interaction between the redox sites (Pt) and storage-release or acid–base sites (Ba-containing particles). Changes in the relationship between these two kinds of sites may be responsible for reduced efficiency of the NO_x trap after aging. To probe these interactions at the molecular level, we have prepared fresh and thermally aged $Pt/Ba/Al_2O_3$ catalysts and used *in situ* UV and visible Raman spectroscopy.

We have observed certain Raman features to be present, absent, or to change in nature in these $Pt/Ba/Al_2O_3$ catalysts depending on aging temperature and Raman excitation wavelength. These features are due to oxygen species on Pt, physisorbed H_2O on Al_2O_3, and various NO_x species. We have observed these species in previous Raman studies [11,16,17] and the results of this current work will draw heavily on those. Our observations show that interactions between Pt, Ba-containing particles, and Al_2O_3 in the catalyst have changed after aging. More specifically, the individual components have sintered and are farther apart in the aged catalyst, which could disrupt the smooth transition between the redox and acid–base functions and result in a lower efficiency.

*To whom correspondence should be addressed.
E-mail: duy@ford.com

1011-372X/04/0600–0191/0 © 2004 Plenum Publishing Corporation

2. Experimental

2.1. Sample preparation and aging

Fumed γ-Al_2O_3 (Alfa Aesar) was stirred into deionized H_2O until suspended. 18 wt% Ba as $Ba(NO_3)_2$ was then deposited into the suspension, and the resulting paste oven dried at 50 °C overnight and calcined at 600 °C for 6 h in 6%O_2-enriched air. 2 wt% Pt as $H_2PtCl_6{\cdot}6H_2O$ was then added and the resulting solution milled for 24 h, dried, and calcined at 600 °C for 6 h in 6%O_2-enriched air. This is the "fresh" catalyst. The "aged" catalysts are the "fresh" $Pt/Ba/Al_2O_3$ samples heated to specified higher temperatures for an additional 8 h in the O_2-enriched air. Samples were cooled in the O_2-enriched air.

2.2. Raman

Raman spectra were collected using a Renishaw 1000 Raman Microscope system with dual wavelength capability in the UV (244 nm) and the visible (488 nm) [18,19]. Kinematic optics modules optimized for either UV or visible operation allowed fast (~15 min) switching between the two wavelengths. Holographic notch filters attenuated the Rayleigh scatter for visible-excited spectra, whereas stacked dielectric filters were used for the UV-excited spectra. The former allowed Raman spectra to be obtained to within 100 cm^{-1} of the Rayleigh line, the latter to within 400 cm^{-1} of the Rayleigh line. The resolution of the 488 nm spectra is ~3 cm^{-1}, whereas it is ~ 8 cm^{-1} for the 244 nm spectra. The Si peak at 521 cm^{-1} and the single-crystal graphite peak at 1582 cm^{-1} were used to calibrate the visible and UV Raman spectra, respectively.

In situ experiments were conducted using a Linkam TMS1500 heating stage that allowed the flow of gases over the sample. Either ~0.5 mg of the powdered sample was used directly, or pressed into 3 mm pellets weighing ~10 mg. No difference was observed in the Raman results; the pellet pressing was meant to facilitate focusing onto the sample. At the beginning of each experimental run, the sample was pretreated in the Linkam stage as follows: heated in O_2 to 500 °C at 10°/min, kept at 500 °C for 20 min each in O_2 then 5% H_2, then cooled in 5% H_2 at 10°/min to the desired temperature. The gas mixtures used were (a) 50 sccm of 500 ppm NO and 6% O_2 in N_2, (b) 50 sccm 5% H_2 in N_2 and (c) 25 sccm O_2. Since the laser sampled areas with ~10 μm diameters and the catalysts appeared inhomogeneous on this scale, numerous spectra were obtained to ensure reproducibility of results.

Note that Raman intensities observed on heterogeneous catalysts may not be proportional to the concentration of species being observed. In general, Raman scattering cross sections can change as a function of temperature, treatment, particle size, crystallinity, and sample thickness [20–24]. Raman spectra obtained by either UV or visible excitation have the same selection rules, but resonance enhancement (where the excitation frequency corresponds to an electronic transition in the material) or photochemical effects by the UV can create differences in the observed spectra. Awareness of these possibilities is necessary for drawing appropriate conclusions from the Raman results.

2.3. BET, chemisorption, and X-ray diffraction measurements

Adsorption and X-ray diffraction measurements were performed to determine surface areas and sintering behavior of the $Pt/Ba/Al_2O_3$ components as a function of aging and to confirm the Raman results. The Brunauer–Emmett–Teller (BET) method was used to determine the total surface area. H_2 and CO_2 chemisorption measurements were used to determine dispersion of Pt and BaO, respectively.

BET–BET surface areas were measured using a Micromeritics TriStar with ultrapure N_2 at 77 K. The powders were first thoroughly degassed at 300 °C.

H_2 and CO_2 chemisorption – The chemisorption measurements were performed using a Micromeritics ASAP 2010 C volumetric adsorption apparatus. The samples were first oxidized in pure O_2 at 300 °C for 60 min, followed by reduction in H_2 at 700 °C for 30 min. The samples were then evacuated at 300 °C for 5 h, cooled to 35 °C, and analyzed by H_2 or CO_2 chemisorption. X-ray diffraction – X-ray diffraction (XRD) patterns were obtained using a Scintag X2 $\theta:\theta$ diffractometer equipped with a copper target X-ray tube and a thermoelectrically-cooled Li-drifted silicon detector discriminating for CuK_α radiation. The divergence was 1.43°, and the acceptance angle was 0.07°. Data were recorded over a 2θ range from 5 to 90°.

2.4. NO_x storage efficiency measurement

NO_x storage efficiency was measured with a flow reactor coupled to a V&F Airsense 2000 chemi-ionization mass spectrometer. The quartz reactor is 5 mm in diameter. Catalyst powders were pressed into pellets and then crushed to form particles sieved to 40–60 mesh (250–425 μm). In each test, 100 mg of the powder was mixed with 200 mg of 40–60 mesh cordierite powder to minimize temperature changes during the measurement. The sample was first conditioned under a reducing environment at 600 °C for 30 min. After the conditioning, the storage activity was measured at different temperatures with feed gas cycling between lean and rich modes with 60 s in lean and 20 s in rich. The lean feed gas contained 500 ppm NO, 10% CO_2, 10% H_2O, and 6% O_2 in N_2 while the rich contained 4% CO–H_2 (in a 3 : 1 molar ratio) in N_2. The total flow rate was 750 mL/min. The storage efficiency is the ratio between the integrated emitted NO and the total input NO over the 60 s lean period.

2.5. NO oxidation activity

With the previous set-up, oxidation activities of the fresh and aged catalysts to convert NO to NO_2 were also measured. After a preconditioning treatment as described above, the feedgas was switched to the lean composition (500 ppm NO, 6% O_2, 10% CO_2, 10% H_2O, and balance N_2), and the temperature was ramped down from 600 °C to 100 °C. The oxidation efficiency can be calculated either from the disappearance of NO or the formation of NO_2. It has been verified that both calculations result in the same oxidation efficiency. The values reported here are calculated from the disappearance of NO.

3. Results and discussion

3.1. Characteristics of the fresh and aged $Pt/Ba/Al_2O_3$

Figure 1a–c shows the results of the adsorption experiments performed on the fresh and aged $Pt/Ba/Al_2O_3$ samples. A gradual loss of BaO and total surface areas can be deduced from the decreasing uptake of CO_2 and N_2, respectively, as the samples are aged at progressively higher temperatures. This contrasts with the dramatic loss in the surface area of Pt (figure 1b). Dispersion of Pt calcined at 600 °C (fresh) and aged at 800, 850, and 900 °C are calculated to be 41.5, 5.9, 1.8, and 1.5%, respectively. This is consistent with XRD results (figure 1d), where the XRD pattern for the 900 °C-aged $Pt/Ba/Al_2O_3$ showed strong, sharp peaks due to highly crystalline Pt whereas none were visible in the fresh. Other strong peaks in both samples belonged to $BaCO_3$ and γ-Al_2O_3. Faint peaks of $Ba(NO_3)_2$ were also present in the fresh catalyst. Figure 2 shows that NO_x storage efficiency of $Pt/Ba/Al_2O_3$ drops with aging temperature, indicating thermal deactivation.

Figure 3 shows UV (a) and visible (b) Raman spectra of these samples, "as received". The main spectral features observed are: a broad peak near 600 cm^{-1} and a strong, narrow peak at 1060 cm^{-1} in both sets of spectra; the peaks near 3550 and 3700 cm^{-1} in the UV Raman spectra; and a small, broad peak at 330 cm^{-1} in the visible Raman spectra of the less aged catalysts. It is clear that these features, identified below, behave differently depending on the aging temperature and the excitation wavelength used.

- The broad peak at 600 cm^{-1} has been previously assigned to the Pt–O stretch of atomic oxygen adsorbed on step and defect sites of Pt. We previously observed this in UV Raman spectra of Pt/Al_2O_3 [17] and $Pt/Ba/Al_2O_3$ [11] under oxygen environments. (Samples were "fresh" in both cases.) This peak was easily formed and reduced at room temperature [17], consistent with it being more "atomic" or "chemisorbed" instead of "oxidic" or "strongly bound", as referred to in surface science literature [25,26]. In figure 3b, this peak disappears with aging under visible excitation. Under UV excitation, however, it broadens and shifts to higher frequency as aging temperature increases (figure 3a). These differences indicate that atomic oxygen may not be the only species contributing to the Raman peak near 600 cm^{-1} as aging temperature changes.

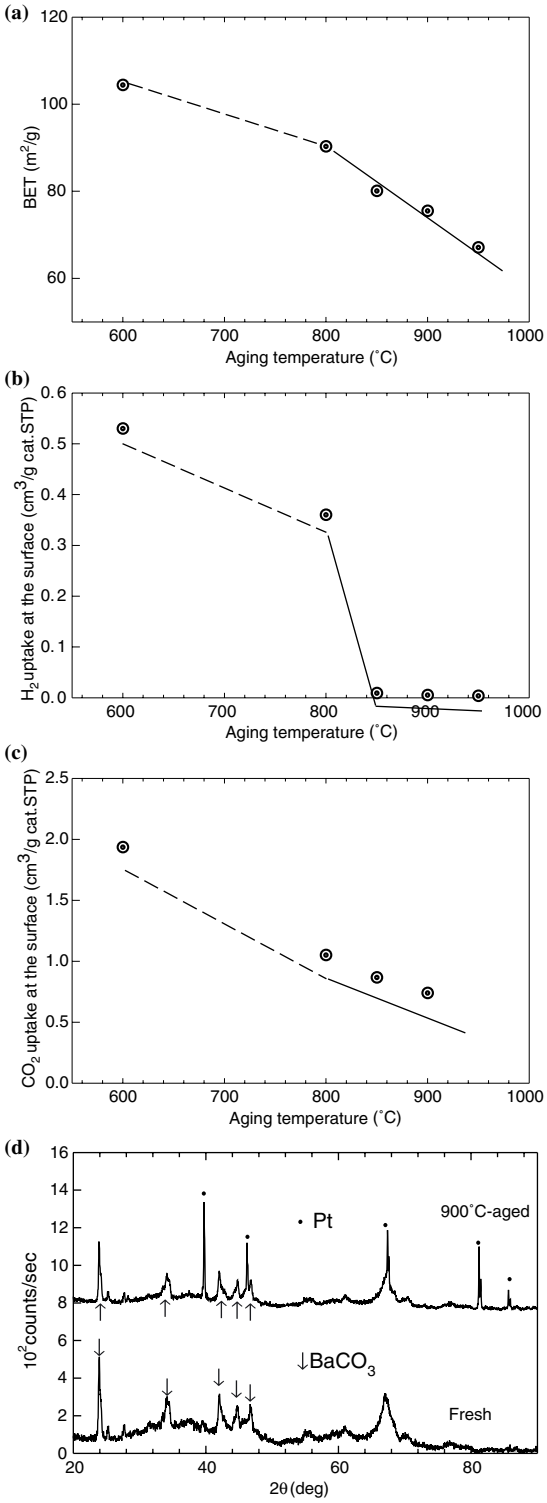

Figure 1. (a) N_2 adsorption, (b) H_2 chemisorption, and (c) CO_2 chemisorption results for fresh and thermally aged $Pt/Ba/Al_2O_3$ catalysts. (d) XRD data for fresh and 900 °C-aged $Pt/Ba/Al_2O_3$.

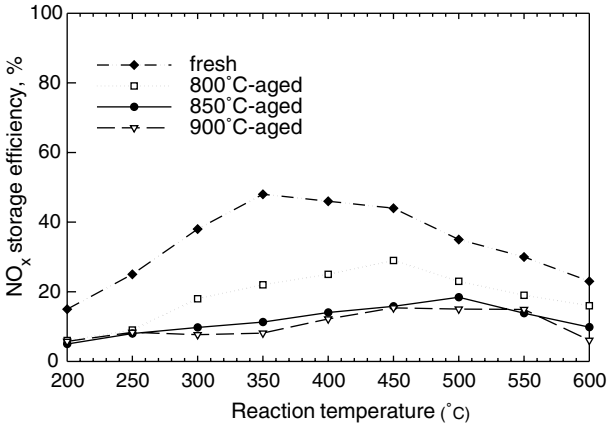

Figure 2. NO_x storage efficiency of fresh and thermally aged $Pt/Ba/Al_2O_3$ at various reaction temperatures.

- The peaks near 3550 and 3700 cm^{-1} under UV excitation belong to O–H stretches on γ-Al_2O_3 [16]. The 3700 cm^{-1} stretch is due to chemisorbed hydroxyls intrinsic to γ-Al_2O_3 [27–29] and is observed in all samples regardless of aging. The stronger, broader band at 3550 cm^{-1} in the more aged samples is from physisorbed H_2O.
- The strong narrow peak at 1060 cm^{-1} belongs to the symmetric C–O stretch of the carbonate ion in $BaCO_3$ [30,31]. Additional peaks belonging to this species are observed in the visible Raman spectra (figure 3b) at 693, 155 and 139 cm^{-1}. Their intensities barely change with aging temperature; however, the 1060 cm^{-1} peak in figure 3a under UV excitation grows significantly upon aging. In the rest of the paper, the nature of Ba-containing particles will be discussed in connection with NO_x species from *in situ* nitration, because we have observed that the amount and nature of $BaCO_3$ in these "as received" catalysts depend on the amount of time the catalyst is exposed to air.
- Finally, the 330 cm^{-1} peak in the fresh $Pt/Ba/Al_2O_3$ is identified as a NO_x species that may require both Pt and Ba-containing particles within close proximity to form, as discussed further in Section 3.5.

These features, along with their variation as a function of excitation wavelength and aging temperature and what they indicate, are listed in table 1. They are discussed more fully in the following sections.

3.2. Atomic oxygen on Pt

Since the behavior of the ~600 cm^{-1} peak in figure 3 varied with excitation wavelength, it was necessary to confirm its identity under both UV and visible excitation. Atomic oxygen is easily reduced at room temperature [25] as shown in our previous UV Raman work on Pt/Al_2O_3 [17]. Thus fresh $Pt/Ba/Al_2O_3$ was subjected to successive flows of either O_2 or NO_2 and 5% H_2 at 25 °C every 30 min. Visible Raman spectra were recorded (figure 4). Under O_2 or NO_2 flow, a broad peak near 600 cm^{-1} formed (figure 4b), which mostly disappeared within minutes of flowing H_2 (figure 4c), and completely disappeared when a second spectrum in H_2 is obtained (not shown). These spectra prove the 600 cm^{-1} peak in visible Raman spectra is indeed atomic O on Pt.

Other peaks in figure 4 under NO_2 flow belong to adsorbed NO_x species, as previously observed on Pt/Al_2O_3 [17]. They are mostly removed by H_2 at 25 °C as well. The 1050 and 734 cm^{-1} peaks correspond to the symmetric N–O stretch and degenerate "bending" mode of the free nitrate ion [30]. The 330 cm^{-1} peak will be discussed further in Section 3.5.

Figure 5 depicts the behavior of atomic O as a function of aging temperature. Visible Raman spectra for the fresh and aged $Pt/Ba/Al_2O_3$ were obtained under O_2 flow at 350 °C, a temperature at which the NO_x trap shows optimum efficiency. All spectra were featureless

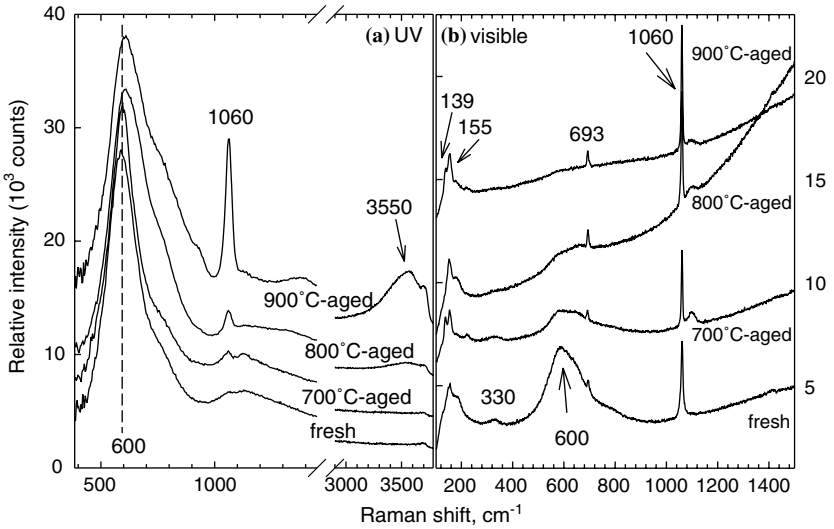

Figure 3. (a) UV and (b) visible Raman spectra of fresh and thermally aged $Pt/Ba/Al_2O_3$.

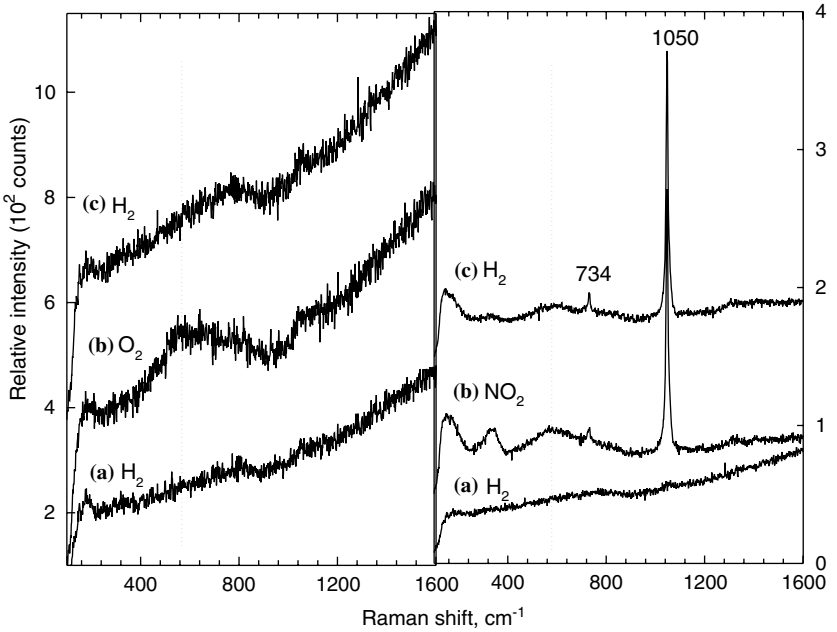

Figure 4. Visible Raman spectra of fresh $Pt/Ba/Al_2O_3$ at 25 °C taken at ~30 min intervals under different flow conditions: (a) 5% H_2, (b) 25 sccm O_2 (left) or 500 ppm NO_2 (right), and (c) 5% H_2. Dotted lines indicate the Pt–O stretch frequency; the 1050 and 734 cm^{-1} peaks are due to the nitrate ion.

prior to O_2 exposure. Under O_2 flow, the 600 cm^{-1} peak immediately appeared in the less aged catalysts. Its disappearance with increasing aging temperature demonstrates the loss of Pt activity, probably due to sintering. As Pt dispersion decreases, fewer sites become available for O_2 adsorption and dissociation.

However, this may not account for all the changes occurring with Pt as the broad peak near 600 cm^{-1} peak appeared in all the $Pt/Ba/Al_2O_3$ samples under UV excitation (figure 3a). Another species, resonantly enhanced by 244 nm excitation and with the following characteristics, is likely present: (a) not enhanced by 488 nm excitation and thus absent in the visible Raman spectra of aged $Pt/Ba/Al_2O_3$; (b) has a peak broader and at slightly higher frequency relative to the atomic oxygen peak; (c) formed under higher aging temperatures; and (d) has a different reduction behavior.

Figure 6 illustrates this last point, which has series of UV Raman spectra of the fresh and 900 °C-aged catalysts at 350 °C. After pretreatment, samples were briefly exposed to O_2 to generate the 600 cm^{-1} peak as shown in the spectra obtained at 0 s in figure 6a and b. After 120 s, H_2 was introduced. The peak disappeared completely after 120 s of H_2 flow in the fresh sample, but still remained after several spectral accumulations in the aged catalyst. The peak in the aged catalyst had the following additional characteristics: incomplete reduction during the H_2 portion of the pretreatment at 500 °C (although mostly reduced at 500 °C when exposed to H_2 in a temperature ramp from 25–500 °C) and slower growth to maximum intensity from a reduced state compared to the fresh catalyst.

The ~600 cm^{-1} peak in the aged $Pt/Ba/Al_2O_3$ has behavior consistent with a strongly bound oxygen on platinum or platinum oxide species observed on Pt surfaces [25,26,32,33], which formed above 500 °C in an O_2 atmosphere and was unreactive even at 720 °C in H_2 or CO. It can clearly coexist with atomic oxygen [26] as shown in figures 3a and figure 6b. In figure 3a, the peak is broader and shifted from the peak in the fresh, and in figure 6b, a portion of the peak disappears (the atomic O part) and leaves a small peak behind (the oxide). Both fresh and aged $Pt/Ba/Al_2O_3$ likely have varying proportions of the chemisorbed and the more strongly bound forms of oxygen, with aging temperature determining the amount of each species. The paper by Somorjai [25] clearly describes the characteristics of these two oxygen species on Pt. While catalyst literature abounds with references to platinum oxides on supported Pt catalysts [34–38], these species were largely ''oxidized'', reduced, or decomposed at lower temperatures. But for nanometer-sized, supported Pt particles, most of the Pt atoms are surface atoms, so there is no clear distinction between a particle that is completely oxidized and one in which only the surface is covered with atomic O [17].

We thus conclude that thermal deactivation of precious metal Pt involves both sintering and high-temperature oxide (or stronglybound oxygen) formation. As Pt sinters and more platinum oxide forms, which is less reactive than atomic O, fewer sites become available for NO and O_2 adsorption and reaction. This

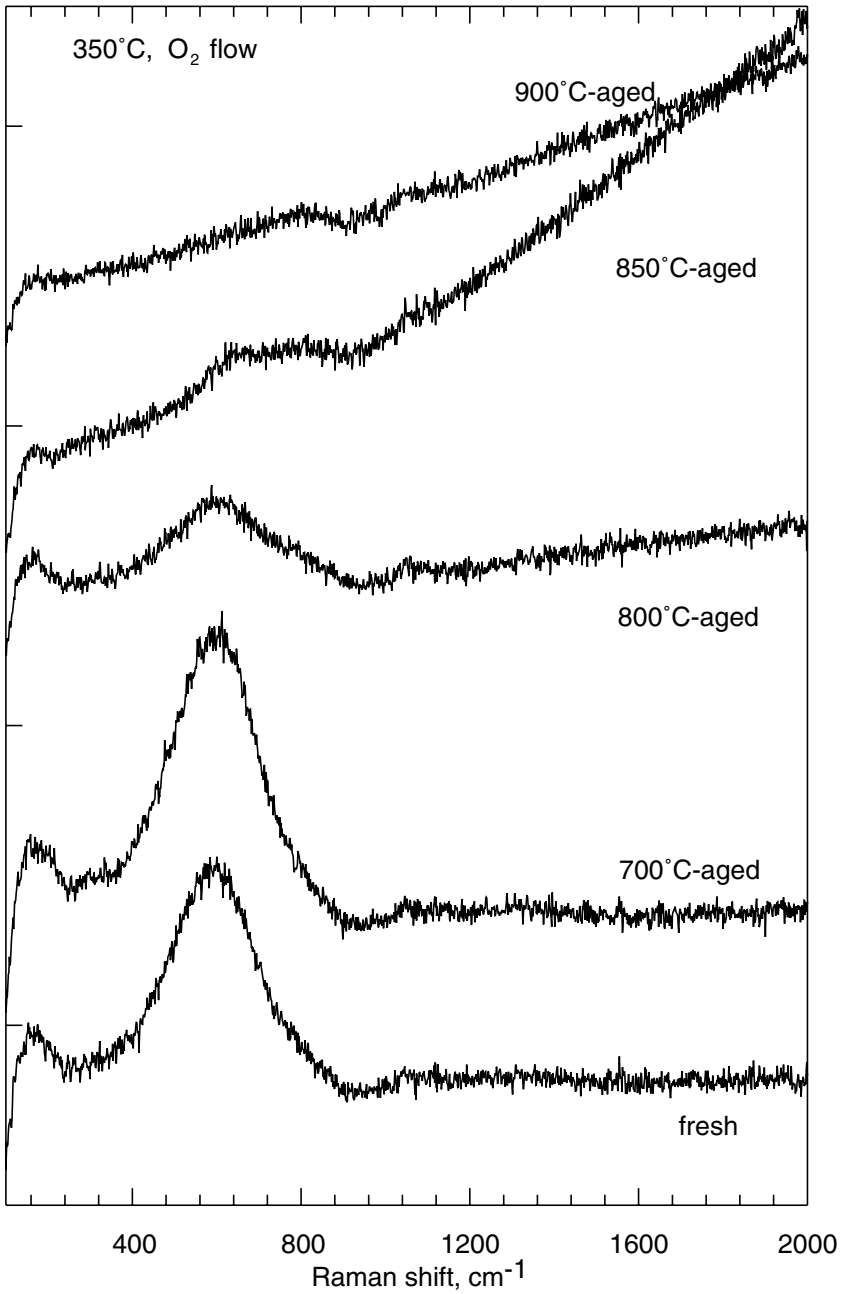

Figure 5. Visible Raman spectra of fresh and aged $Pt/Ba/Al_2O_3$ at 350 °C in 25 sccm O_2 showing the atomic O peak on Pt disappearing with aging temperature.

coincides with a decrease in NO oxidation efficiency in the aged $Pt/Ba/Al_2O_3$ sample as shown in figure 7.

3.3. *Physisorbed H_2O on γ-Al_2O_3*

From infrared spectroscopy, γ-Al_2O_3 is known to have several hydroxyl bands [27–29]. OH stretches are normally difficult to see with Raman, but we found these are enhanced when UV excitation is employed. On γ-Al_2O_3, we have observed OH bands due to both physisorbed H_2O ($\sim$3500 cm^{-1}), which disappears at $\sim$100 °C, and hydroxyls ($\sim$3700 cm^{-1}) (figure 8b) [16]. However, when γ-Al_2O_3 was impregnated with Pt, no OH stretches were observed at ambient conditions, as shown in figure 8a. We do not completely understand this phenomenon, but as we mentioned in Ref. [16], we may observe only a fraction of the possible bands of physisorbed H_2O and chemisorbed hydroxyls on the γ-Al_2O_3, and they reside in sites that are resonantly enhanced with the 244 nm excitation. These, then, are the sites that Pt binds to, blocking the OH Raman signals.

As observed in figure 3a, OH bands get bigger when $Pt/Ba/Al_2O_3$ is aged at higher temperatures. Initially, the OH region of fresh $Pt/Ba/Al_2O_3$ resembles that of Pt/

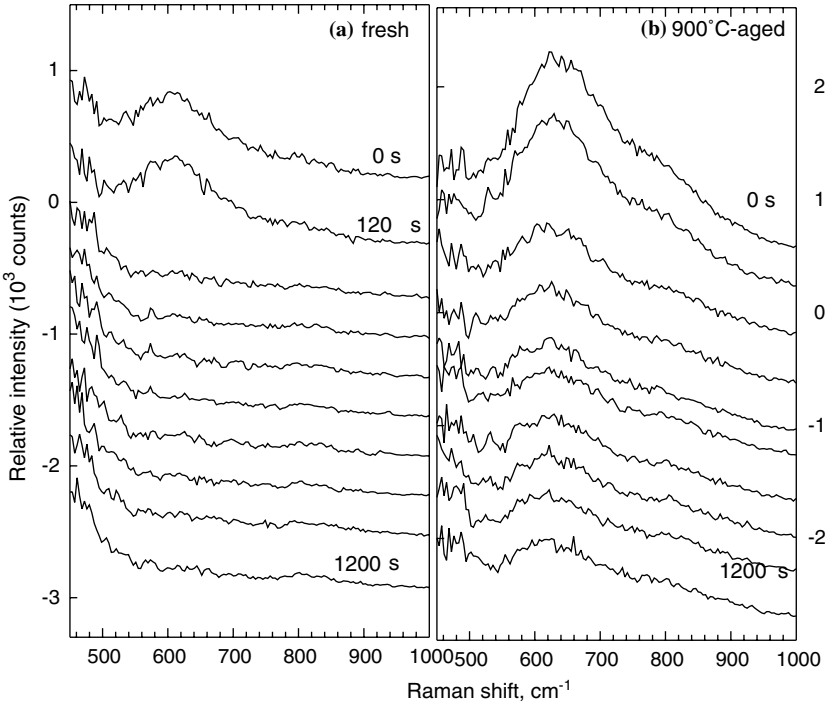

Figure 6. UV Raman spectra of a) fresh and b) 900 °C-aged $Pt/Ba/Al_2O_3$ at 350 °C. The first spectra (0 s) were obtained under exposure to 500 ppm NO and 6% O_2. 5% H_2 was introduced after 120 s.

Al_2O_3, but after aging, it resembles γ-Al_2O_3 (figure 8). Thus it appears that Pt is "separating" from the Al_2O_3 in aged $Pt/Ba/Al_2O_3$. Apparently, while the finely dispersed Pt in the fresh catalyst blocks the resonantly enhanced OH sites, the sintered Pt in the aged catalyst does not.

We know this effect is due to Pt, since the UV Raman spectrum of 5 wt% Ba/Al_2O_3 is similar to γ-Al_2O_3 (not

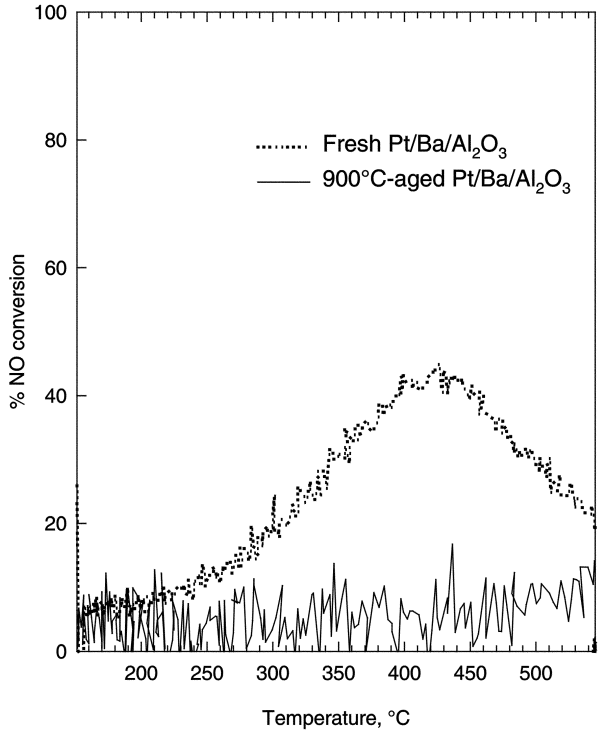

Figure 7. NO oxidation to NO_2 of fresh and 900 °C-aged $Pt/Ba/Al_2O_3$.

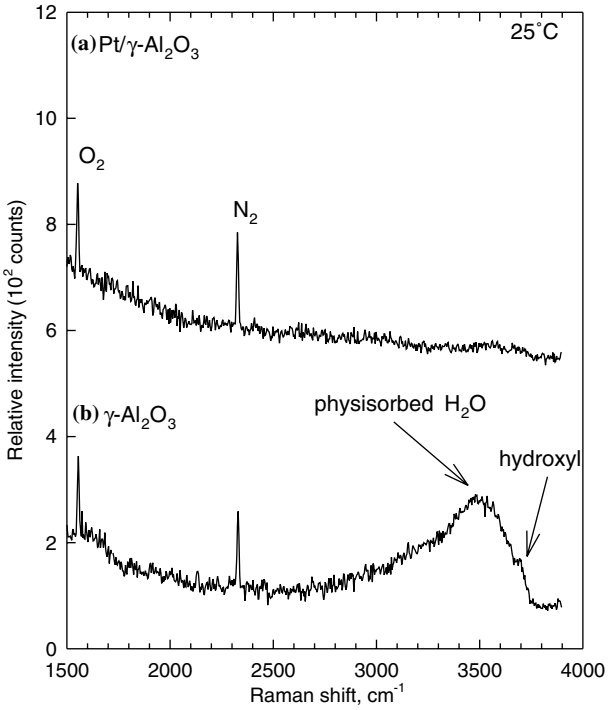

Figure 8. UV Raman spectra of (a) Pt/γ-Al_2O_3 and (b) γ-Al_2O_3 in the OH stretch region obtained under ambient conditions. The O_2 and N_2 peaks are from air.

shown), with both physisorbed H_2O and hydroxyl peaks. FTIR results of other workers [39,40] have mentioned that Ba blocks most of the hydroxyl bands of γ-Al_2O_3 in Ba/Al_2O_3 or $Pt/Ba/Al_2O_3$ and gives a basic character to the support, but this does not contradict our results. We address primarily the physisorbed H_2O band, and we see only two [16], at most, of the 5 or more hydroxyl peaks reported in IR [27–29].

3.4. *Ba nitrate, nitrite/nitro species, and adsorbed NO on Pt*

Figures 9 and 10 show UV and visible Raman spectra, respectively, of fresh $Pt/Ba/Al_2O_3$, 900 °C-aged $Pt/Ba/Al_2O_3$ and fresh Pt/Al_2O_3 (UV only) at 350 °C under flowing NO + O_2. Features observed are due to the symmetric N–O stretch of an ionic-type nitrate at ~1050 cm^{-1} [30] from $Ba(NO_3)_2$ in $Pt/Ba/Al_2O_3$ spectra, the symmetric N–O stretch of nitrite/nitro species at 1320 cm^{-1} [30] and N–O stretch of adsorbed NO on atop sites of Pt at 1730 cm^{-1} [41] in 900 °C-aged $Pt/Ba/Al_2O_3$ (figure 9a) and Pt/Al_2O_3 (figure 9c), and another NO_x species at 310 cm^{-1} in fresh $Pt/Ba/Al_2O_3$ (figure 10). The latter will be discussed in Section 3.5.

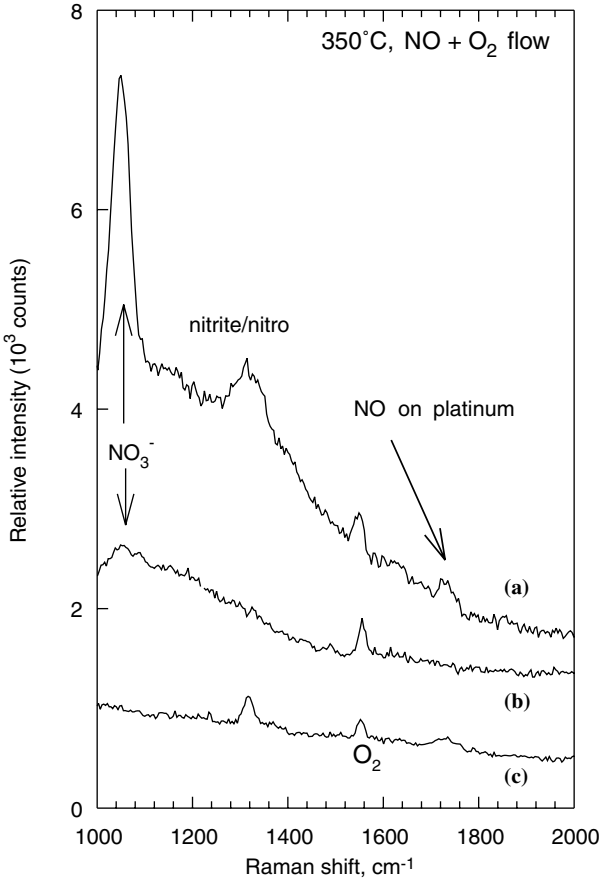

Figure 9. UV Raman spectra of (a) 900 °C-aged $Pt/Ba/Al_2O_3$, (b) fresh $Pt/Ba/Al_2O_3$ and (c) Pt/Al_2O_3 at 350 °C under 500 ppm NO + 6%O_2 flow.

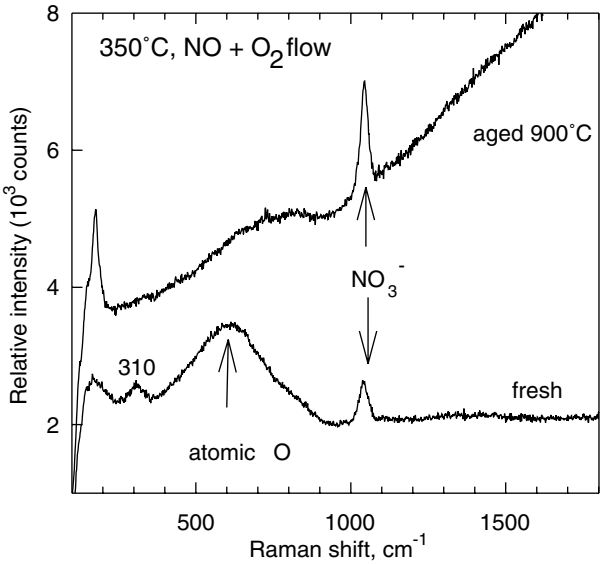

Figure 10. Visible Raman spectra of fresh and 900 °C-aged $Pt/Ba/Al_2O_3$ at 350 °C under 500 ppm NO + 6%O_2.

From figure 9, we see that fresh and aged $Pt/Ba/Al_2O_3$ have dissimilar spectra. The nitrate peak is still present, but is more intense in the aged. The aged $Pt/Ba/Al_2O_3$ spectrum also shows nitrite/nitro species and adsorbed NO, which makes it similar to the fresh Pt/Al_2O_3 spectrum (figure 9c).

Our studies on fresh and 1050 °C-aged Pt/Al_2O_3 have shown that the same NO_x species form on Al_2O_3 under NO + O_2 flow at 300 °C. These results show that the similarity of the 900 °C-aged $Pt/Ba/Al_2O_3$ spectrum to Pt/Al_2O_3 under NO + O_2 flow is not due to aged Pt or aged Al_2O_3 but is more consistent with Ba-containing particles behaving somewhat independently of (or "separating" from) Pt/Al_2O_3.

This "separation" is supported by the decrease in dispersion of BaO_x with aging temperature (figure 1c), Pt "separating" from Al_2O_3 in aged $Pt/Ba/Al_2O_3$ (Section 3.3) and the appearance of the 330 cm^{-1} peak in fresh but not in aged $Pt/Ba/Al_2O_3$ (Section 3.5) However, this "separation" is not complete. A fraction of barium-containing particles is still "associated" with Pt because barium nitrate formed in aged $Pt/Ba/Al_2O_3$. The nitrate peak in the aged $Pt/Ba/Al_2O_3$ catalyst is actually bigger than in the fresh, but this is due to the $Ba(NO_3)_2$ particles being more crystalline, and not to a greater quantity of $Ba(NO_3)_2$ being formed. This crystallinity can be deduced from the spectra in two ways: through the linewidth, intensity, and frequency of the nitrate peaks; and through photo-induced formation of nitrite under UV excitation, as discussed in the following paragraphs.

Figure 2 shows that NO_x storage is largest in the fresh catalyst. If we believe storage occurs primarily in

the form of $Ba(NO_3)_2$, then this is inconsistent with figures 9 and 10 showing a bigger nitrate peak in aged $Pt/Ba/Al_2O_3$. Aside from bring more intense in aged $Pt/Ba/Al_2O_3$, the nitrate peak is ~15% narrower and, on average, ~4 cm^{-1} higher in frequency than in the fresh catalyst under visible excitation (figure 10). Studies on CeO_2 dispersed on γ-Al_2O_3 have shown a relationship between linewidth, intensity, and crystallite size; the CeO_2 peak red-shifts and broadens with decreasing crystallite size [42,43]. Thus, the intensity, width, and frequency of the $Ba(NO_3)_2$ peaks suggest more crystalline $Ba(NO_3)_2$ particles exist in aged $Pt/Ba/Al_2O_3$ than in the fresh.

It may be noticed that the carbonate peaks at 1060 cm^{-1} from figure 3b (under visible excitation) do not shift to higher frequency with increasing aging temperature, as the nitrate peak does during the *in situ* nitration in figure 10. (The width does decrease, but this is not apparent in the figure.) This is because the barium carbonate is already somewhat crystalline to begin with, as shown by the presence of the phonon modes at 139 and 155 cm^{-1} in all the samples and their relatively narrow peaks compared to those of other species discussed. As we mentioned earlier, $BaCO_3$ spontaneously forms when BaO is exposed to air, its nature changing with length of exposure to air and high temperature. Thus, it is more reliable to probe the condition of barium during *in situ* nitration, after the catalysts have undergone similar pretreatment.

However, the $CO_3^=$ peak under UV excitation (figure 3a) does get more intense with aging temperature. Apparently, UV Raman is still sensitive to particle crystallinity as shown here by the variations in peak intensity.

The other phenomenon that indicates crystallinity of the $Ba(NO_3)_2$ particles is photo-induced nitrite formation under UV excitation. It is known that UV light can induce the formation of nitrites from crystalline nitrates [44,45], and the $Ba(NO_3)_2$ in aged $Pt/Ba/Al_2O_3$ may be crystalline enough for this to happen. In figure 9a, the nitrite/nitro peak in aged $Pt/Ba/Al_2O_3$ is broad compared to the corresponding peak in the Pt/Al_2O_3 spectrum (figure 9c), and thus may be associated not just with Al but also with Ba ions.

We can verify photo-induced nitrite formation can occur under our UV excitation by comparing UV and visible Raman spectra of bulk crystalline $Ba(NO_3)_2$ as shown in figure 11. The most intense nitrate lines under visible excitation (figure 11a) correspond to the symmetric N–O stretch at 1050 cm^{-1}, the degenerate bending mode at 734 cm^{-1}, and a lattice mode at 143 cm^{-1}. The UV Raman spectrum (figure 11b), on the other hand, has the following prominent peaks: 815, 1050, 1320, 1637, 2090, 2630 cm^{-1} with the peaks at 815 and 1320 cm^{-1} corresponding to fundamental vibrations of the nitrite ion . The peak at 2630 cm^{-1} is also from

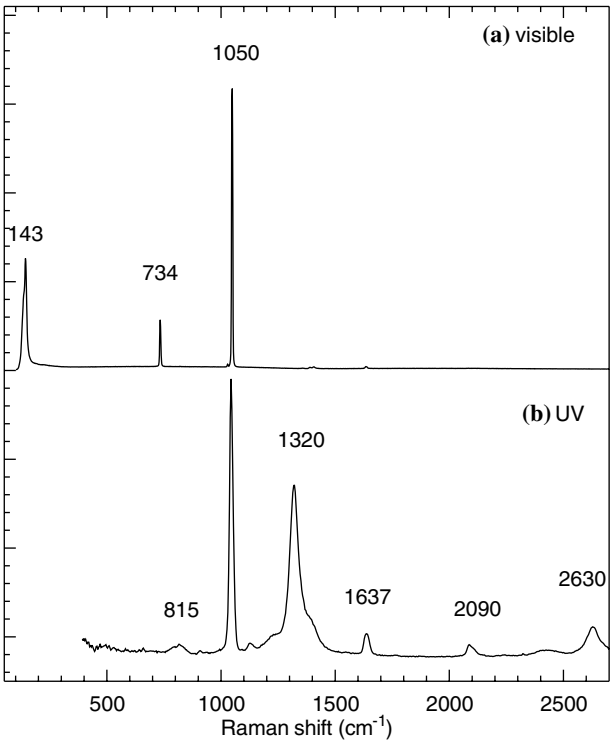

Figure 11. Raman spectra of $Ba(NO_3)_2$ obtained under (a) visible and (b) UV excitation.

nitrite and is the first overtone of the 1320 cm^{-1} peak. (The peaks at 1637 and 2090 cm^{-1} are from nitrate.)

3.5. NO_x species on $Pt/Ba/Al_2O_3$

The last feature characteristic of the fresh but not aged $Pt/Ba/Al_2O_3$ is the peak appearing at ~310 cm^{-1} at 350 °C (figure 10) and at ~330 cm^{-1} at 25 °C (figures 3 and 4). It is associated with a nitrogen or NO_x species since it is observed under NO + O_2 or NO_2 flow but not under O_2 flow. (It is present in the "as received" samples but we have occasionally observed NO_x species on "as received" catalysts, which may have been contaminated from handling or from the nitrate precursor.) It is a surface species because it is readily formed and removed at 25 °C as shown in figure 4. The peak does not form on Pt/Al_2O_3, Ba/Al_2O_3, and γ-Al_2O_3 under NO_2 flow.

From literature , a peak near 330 cm^{-1} can be attributed to a Raman-active metal–NO_2 stretch. However, it cannot purely be metal–NO_2 in our case, otherwise we should observe the symmetric N–O stretch of NO_2 at ~1320 cm^{-1} in the fresh $Pt/Ba/Al_2O_3$, and we do not. Labalme *et al.* have reported a CO species bridge-bonded onto Pt and Ba particles in fresh $Pt/Ba/Al_2O_3$ catalysts . Perhaps the ~330 cm^{-1} NO_x species on fresh $Pt/Ba/Al_2O_3$ has a similar nature but at this point we cannot positively ascertain its identity, or confirm its role in the NO_x storage process. Further experiments are under way to address this issue.

Table 1
Summary of Raman features indicating thermal deactivation in aged $Pt/Ba/Al_2O_3$

Excitation λ, nm	Species	Fresh $Pt/Ba/Al_2O_3$	Aged $Pt/Ba/Al_2O_3$	
488	Atomic O on Pt, $\sim$600 cm^{-1}	Present	Absent	Loss coincides with decreasing NO oxidation activity
244	High temperature platinum oxide, $\sim$600 cm^{-1}	Absent	Present	Presence coincides with decreasing NO oxidation activity
244	Physisorbed H_2O, 3550 cm^{-1}	Absent	Present	Separation of Pt from γ-Al_2O_3
244 and 488	$Ba(NO_3)_2$, 1050 cm^{-1}	Broad and weak	Strong, narrow, and blue-shifted	Ba-containing particles becoming more crystalline
244	Nitrite/nitro species, $\sim$1320 cm^{-1}	Absent	Associated with γ-Al_2O_3 and possibly Ba (photo-induced by crystalline $Ba(NO_3)_2$)	Separation of Ba-containing particles from Pt/Al_2O_3
244	NO on Pt, $\sim$1730 cm^{-1}	Absent	Present	Separation of Ba-containing particles from Pt/Al_2O_3
488	NO_x species needing Pt and Ba, $\sim$330 cm^{-1}	Present	Absent	Possible loss of proximity of Pt and Ba-containing particles

4. Summary

We have shown how the presence, absence, or nature of certain features in UV and visible Raman spectra of $Pt/Ba/Al_2O_3$ illustrate how thermal deactivation occurs when the catalyst ages. The Raman results indicate that sintering and separation of components have occurred in the aged catalysts, consistent with data from BET, chemisorption, XRD, and activity measurements. The specific Raman features we discussed are enumerated below and in Table 1:

1. Atomic oxygen and strongly bound oxygen on Pt are observed through the Pt–O stretch near 600 cm^{-1} . As aging temperature increases, there is less atomic O but more of the strongly bound, less reactive species formed. This coincides with decreasing NO oxidation activity with aging temperature.
2. The O–H stretch of physisorbed H_2O ($\sim$3550 cm^{-1}) is observed in aged $Pt/Ba/Al_2O_3$ but not in the fresh at ambient conditions. Since the same O–H stretch is seen in spectra of γ-Al_2O_3 but not in Pt/Al_2O_3, this means the Pt is : "separating" from the γ-Al_2O_3 in the aged $Pt/Ba/Al_2O_3$, allowing the OH stretch to be observed.
3. The peak due to the symmetric N–O stretch (1050 cm^{-1}) of $Ba(NO_3)_2$ is more intense, narrower, and higher in frequency in the aged $Pt/Ba/Al_2O_3$ than in the fresh, indicating a larger barium nitrate crystallite size in the aged catalyst. The possible formation of $Ba(NO_2)_2$ under UV excitation on aged $Pt/Ba/Al_2O_3$ is consistent with this crystallinity.
4. Under NO + O_2 flow, the spectrum of aged $Pt/Ba/Al_2O_3$ is similar to that of Pt/Al_2O_3, with nitrite/nitro species ($\sim$1320 cm^{-1}) and NO adsorbed on Pt ($\sim$1730 cm^{-1}). This similarity is consistent with Ba-containing particles "separating from" or behaving independently from the Pt/Al_2O_3.
5. A surface NO_x species appearing in fresh $Pt/Ba/Al_2O_3$ at $\sim$330 cm^{-1} but not in the aged may indicate proximity of Pt and Ba particles in the fresh catalyst.

Acknowledgments

We are greatly indebted to W.H.Weber, W.F. Schneider, G. W. Graham, A. Bogicevic, R.W. McCabe, C. Lowe-Ma, and C.T. Goralski for discussions and helpful criticism.

References

[1] N. Miyoshi, S. Matsumoto, K. Katoh, T. Tanaka, J. Harada, N. Takahashi, K. Yokota, M. Sugiura and K. Kasahara, SAE Paper 950809 (1995).
[2] N. Takahashi, H. Shinjoh, T. Iijima, T. Suzuki, K. Yamazaki, K. Yokota, H. Suzuki, N. Miyoshi, S. Matsumoto, T. Tanizawa, T. Tanaka, S. Tateishi and K. Kasahara, Catal. Today 27 (1996) 63.
[3] D. James, E. Fourré, M. Ishii and M. Bowker, Appl. Catal. B 45 (2003) 147.
[4] B.-H. Jang, T.-H. Yeon, H.-S. Han, Y.-K. Park and J.-E. Yie, Catal. Lett. 77 (2001) 21.
[5] L.F. Liotta, A. Macaluso, G.E. Arena, M. Livi, G. Centi and G. Deganello, Catal. Today 75 (2002) 439.
[6] E. Fridell, H. Persson, B. Westerberg, L. Olsson and M. Skoglundh, Catal. Lett. 66 (2000) 71.
[7] L. Lietti, P. Forzatti, I. Nova and E. Tronconi, J. Catal. 204 (2001) 175.
[8] A.J. Paterson, D.J. Rosenberg and J.A. Anderson, in: *Studies in Surface Science and Catalysis*, eds. A. Guerrero-Ruiz, I. Rodriguez-Ramos (Elsevier Science B.V., 2001) p. 429.
[9] C. Sedlmair, K. Seshan, A. Jentys and J.A. Lercher, J. Catal. 214 (2003) 308.

[10] I. Nova, L. Castoldi, L. Lietti, E. Tronconi and P. Forzatti, Catal. Today 75 (2002) 431.
[11] D. Uy, K.A. Wiegand, A.E. O'Neill, M.A. Dearth and W.H. Weber, J. Phys. Chem. B 106 (2002) 387.
[12] T. Kobayashi, T. Yamada and K. Kayano, SAE Paper 970745 (1997).
[13] F. Rodrigues, L. Juste, C. Potvin, J.F. Tempère, G. Blanchard and G. Djèga-Mariadassou, Catal. Lett. 72 (2001) 59.
[14] H. Mahzoul, J.F. Brilhac and P. Gilot, Appl. Catal. B 20 (1999) 47.
[15] N.W. Cant and M.J. Patterson, Catal. Today 73 (2002) 271.
[16] D. Uy, A. Dubkov, G.W. Graham and W.H. Weber, Catal. Lett. 68 (2000) 25.
[17] D. Uy, A.E. O'Neill and W.H. Weber, Appl. Catal. B 35 (2002) 219.
[18] D. Uy, A.E. O'Neill, L. Xu, W.H. Weber and R.W. McCabe, Appl. Catal. B 41 (2003) 269.
[19] G.W. Graham, A.E. O'Neill, D. Uy, W.H. Weber, H. Sun and X.Q. Pan, Catal. Lett. 79 (2002) 99.
[20] G. Mestl, J. Mol. Catal. A 158 (2000) 45.
[21] F. Vratny and R.B. Fischer, Appl. Spectrosc. 14 (1960) 76.
[22] S. Xie, E. Iglesia and A. Bell, T., J. Phys. Chem. B 105 (2001) 5144.
[23] M.V. Pellow-Jarman, P.J. Hendra and R.J. Lehnert, Vib. Spectrosc. 12 (1996) 257.
[24] D.N. Waters, Spectrochim. Acta 50A (1994) 1833.
[25] C.E. Smith, J.P. Biberian and G.A. Somorjai, J. Catal. 57 (1979) 426.
[26] J.L. Gland, B.A. Sexton and G.B. Fisher, Surf. Sci. 95 (1980) 587.
[27] H. Knözinger and P. Ratnasamy, Catal. Rev.-Sci. Eng. 17 (1978) 31.
[28] J.B. Peri, J. Phys. Chem. 69 (1965) 211.
[29] A.A. Tsyganenko and P.P. Mardilovich, J. Chemi. Soc. Faraday Trans. 92 (1996) 4843.
[30] K. Nakamoto, *Infrared and Raman Spectra of Inorganic and Coordination Compounds. Part A. Theory and Applications in Inorganic Chemistry* (John Wiley & Sons, Inc., New York, 1997).
[31] I.A. Degen and G.A. Newman, Spectrochim. Acta 49A (1993) 859.
[32] H. Niehus and G. Comsa, Surface Sci. Lett. 93 (1980) L147.
[33] T. Matsushima, D.B. Almy and J.M. White, Surf. Sci. 67 (1977) 89.
[34] R.W. McCabe, C. Wong and H.S. Woo, J. Catal. 114 (1988) 354.
[35] O. Alexeev and B.C. Gates, in: *Studies in Surface Science and Catalysis*, Vol. 130, eds. A. Corma, F.V. Melo, S. Mendioroz, J.L.G. Fierro (2000) p. 371.
[36] A. Borgna, F. Le Normand, T. Garetto, C.R. Apesteguia and B. Moraweck, Catal. Lett. 13 (1992) 175.
[37] C.-B. Wang and C.-T. Yeh, J. Catal. 178 (1998) 450.
[38] L. Olsson and E. Fridell, J. Catal. 210 (2002) 340.
[39] F. Prinetto, G. Ghiotti, L. Lietti, E. Tronconi and P. Forzatti, J. Phys. Chem. B 105 (2001) 12732.
[40] V. Labalme, N. Benhamou, N. Guilhaume, E. Garbowski and M. Primet, Appl. Catal. A 133 (1995) 351.
[41] W.A. Brown and D.A. King, J. Phys. Chem. B 104 (2000) 2578.
[42] G.W. Graham, W.H. Weber, C.R. Peters and R. Usmen, J. Catal. 130 (1991) 310.
[43] J.E. Spanier, R.D. Robinson, F. Zhang, S.-W. Chan and I.P. Herman, Phys. Rev. B: Condens. Matter 64 (2001) 245407.
[44] L.K. Narayanswamy, Trans. Faraday Soc. 31 (1935) 1411.
[45] R. Vogt and B.J. Finlayson-Pitts, J. Phys. Chem. 99 (1995) 17269.
[46] D.M. Adams, *Metal-Ligand and Related Vibrations: A Critical Survey of the Infrared and Raman Spectra of Metallic and Organometallic Compounds* (Edward Arnold Ltd, London, 1967).